FISEVIER

Contents lists available at ScienceDirect

Soil Dynamics and Earthquake Engineering

journal homepage: www.elsevier.com/locate/soildyn





Cyclic failure characteristics of silty sands with the presence of initial shear stress

Xiao Wei ^{a,b}, Zhongxuan Yang ^c, Jun Yang ^{d,*}

- ^a Engineering Research Center of Urban Underground Space Development of Zheijang Province, Zheijang University, China
- ^b Research Center of Coastal and Urban Geotechnical Engineering, Zhejiang University, Hangzhou, Zhejiang, China
- ^c Department of Civil Engineering, Zhejiang University, Hangzhou, Zhejiang, China
- d Department of Civil Engineering, University of Hong Kong, Hong Kong, China

ARTICLE INFO

Keywords: Cyclic loading Failure patterns Liquefaction resistance Silty sand Initial shear

ABSTRACT

Liquefaction of silty sands remains an outstanding issue since it continues to lead to catastrophic consequences in recent earthquake events. The cyclic characteristics, such as cyclic failure pattern and cyclic resistance, are the fundamental aspects of liquefaction analysis. The difficulty and uncertainty of characterization and evaluation of cyclic behavior and liquefaction resistance of silty sand mainly come from the complicated interactions of various influencing factors, such as packing density, confining pressure, initial shear stress, cyclic loading amplitude, soil properties, and soil fabric. This study presents a series of laboratory testing results to identify the cyclic failure patterns of silty sands considering different soil states, fines contents, initial static shear stress, etc. It is found that the failure patterns are related to the states of soils and the cyclic loading characteristics, i.e., the combination of initial shear stress and cyclic loading amplitude for silty sands with similar soil fabric, and that the cyclic resistance of silty sands is also a function of soil states and initial static shear stress for similar soil fabric. Critical state soil mechanics is implemented to characterize the cyclic failure patterns and cyclic resistance. Implications of the present study to the existing liquefaction assessment methods are also discussed.

1. Introduction

Soil liquefaction tremendously threatens earth structures during earthquake events and has drawn significant engineering concern since the 1964 Niigata earthquake, but it remains an unsolved problem in both engineering practice and scientific research even after decades of investigations. Identifying cyclic failure patterns and evaluating the cyclic resistance of sand are two fundamental aspects of liquefaction assessment [1]. Previous investigations have revealed that both cyclic failure patterns and liquefaction resistance are influenced by the initial states (i.e., the packing densities and the effective confining pressures) of given sand [2–8]. In addition, the presence of initial static shear stress (τ_s) , which is induced by sloping ground or existing structures (Fig. 1(a) and (b)), can also alter the cyclic resistance and the failure pattern [2,3, 9-14], by changing the characteristics of the seismic stress cycles (Fig. 1 (c)-(e)). However, there is no reliable method to evaluate the cyclic resistance and predict the failure patterns of sands with the presence of initial static shear stress.

Experimental studies based on test data of clean sands have

identified several typical cyclic failure patterns, and found that the packing density of sand and the stress reversal condition of the cyclic loading are two major factors controlling the cyclic failure patterns (e.g., Refs. [11,15–18]). Some researchers also suggested that there could be correlations between the monotonic and the cyclic soil responses, suggesting possible ways to predict the failure pattern of sands subjected to cyclic loadings [10,19]. However, these prediction methods were not comprehensive because most of these studies were based on limited testing conditions and were not able to reveal the complicated interactions among multiple influencing factors (e.g., packing density, effective stress, initial static shear stress, and the stress reversal condition of the cyclic loading).

In practice, the initial static shear stress is usually represented by a dimensionless quantity, known as the initial static shear stress ratio, α , which is calculated by $\alpha = \tau_s/\sigma'_{v0}$ (σ'_{v0} is the initial vertical effective stress). The initial static shear stress may have either beneficial (e.g., Ref. [4]) or detrimental (e.g., Ref. [20]) impacts on the cyclic resistance ratio of sands. Harder and his co-workers [21,22] compiled a database from published literature and suggested positive effects of α for sands

E-mail address: junyang@hku.hk (J. Yang).

^{*} Corresponding author.

with relative densities of 55-70%, negative for sands with relative densities of 35%, and intermediate for medium dense sands (relative density of 45-50%). This proposal has been discussed by the National Center for Earthquake Engineering Research (NCEER) [23], however, NCEER recommended it not be used by non-specialists or in routine engineering practice [23] because of the poor convergence and consistency in the database and analysis. In recent years, continuous investigations further confirmed that the effect of initial static shear stress depends on the packing density and effective stress [2,9,12,24,25]. Boulanger [9] characterized the effects of initial static shear stress on cyclic resistance using the relative state index. Yang and Sze [2,24] proposed a critical state-based framework to characterize the effects of initial static shear stress on the liquefaction resistance of clean sands, with unified and combined consideration of the effects of packing density and effective stress through the state parameter [26]. These investigations also indicated that the effect of initial static shear stress can be influenced by the state of sand. However, Harder's proposal [21,22] did not properly consider the impact of confining pressure on the effects of initial static shear stress on cyclic resistance of sands, and this may partly explain the poor convergence of their proposal.

Because of difficulties in retrieving undisturbed sand samples for laboratory testing, different sample preparation methods were developed to simulate the deposition process of the tested soils aiming to replicate the in-situ soil fabric. Experimental results have indicated the mechanical behaviors of sands are affected by sample preparation methods under otherwise similar conditions [27-29]. Regarding the cyclic behaviors and resistance against liquefaction, the influence of fabric is complicated. In addition to the initial states of sands, experimental investigations have found that specimens reconstituted by different sample preparation methods can have different cyclic failure patterns and cyclic resistance even for the same initial state [11,28,30, 31]. For example, Tatsuoka et al. [32] reported that the cyclic resistance of sand prepared by moist tamping is significantly higher than that of sand prepared by air pluviation when the relative density is larger than 70%, but the cyclic resistance of sand prepared by the two methods remain nearly the same for lower relative densities. Sze and Yang [11] reported that a moist-tamped specimen with a relative density of 50% exhibited cyclic mobility under cyclic loading, but a dry-deposited specimen exhibited a failure pattern known as limited flow followed by cyclic mobility under otherwise similar conditions. Several recent investigations [11,33] indicated that cyclic characteristics of clean sands can be even more complicated when the effects of initial fabric and initial static shear stress were combined. However, it is worth noting

that the existing studies mainly used clean sand specimens consolidated to a zero-initial static shear stress, further investigation is needed for silty sands to take into account the initial fabric and initial static shear stress.

Reconstituted clean sand specimens have been extensively used in laboratory investigations, however, silty sands widely exist in nature and engineering projects. Case histories in recent earthquake events indicate that liquefaction characteristics of silty sands are not yet fully understood [34-37]. Most of these existing studies about silty sands investigated the effects of fines content on the cyclic resistance (e.g., Refs. [38-45]). There appears an agreement that the liquefaction resistance decreases with increasing fines content for silty sands with the same void ratio and confining pressure when the fines content is smaller than a transition fines content [41–43,46,47], given that the transition fines content represents that the micro-structure turns from sand-dominant to fines-dominant [48]. Wei and Yang [49] reported that such a decrease in cyclic resistance due to the addition of fines is primarily related to the size disparity ratio between the coarse and the fine particles. Recently, a series of experiments conducted by Wei and Yang [3] indicated that fines content can alter the effects of initial static shear stress on the cyclic resistance for a given initial state in terms of void ratio and effective stress, while Pan et al. [50] compared the cyclic resistance of clean Fujian sand and its mixture with crushed silt (FC = 10%) for relative density around 40%, and found that the cyclic resistances of the clean and the silty sand are almost the same for a variety of initial static shear stress levels. Nevertheless, most of the previous investigations on liquefaction characteristics of silty sands merely considered complex interactions between the initial static shear stress and the state of sand.

According to the aforementioned literature review, it is of interest to characterize the combined effects of initial static shear stress and soil fabric on the liquefaction characteristics of silty sands with different initial states. This study presents a structured experimental program together with a detailed analysis of the failure patterns and cyclic resistance of silty sands under a variety of initial states of soil and loading conditions. Effects of initial static shear stress and fabric are characterized in the framework of critical state soil mechanics, and implications for practical engineers are also discussed.

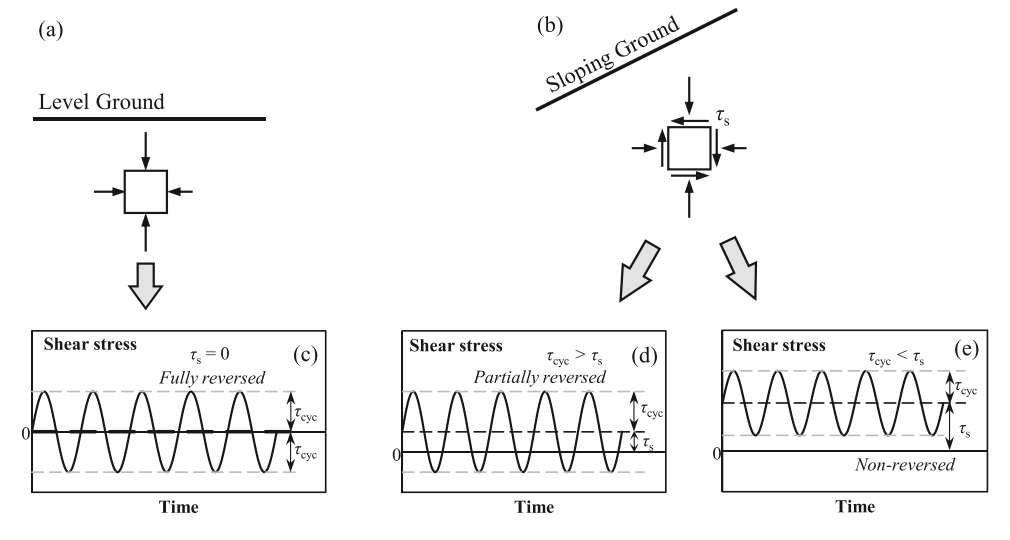


Fig. 1. Presence of initial static shear stress and stress reversal conditions.

2. Experimental program

2.1. Materials

Toyoura sand (TS) is uniform silica sand that consists of mainly subangular particles, and it has been widely used in studies about soil liquefaction. In this study, non-plastic crushed silica fines, with angular particle shape, were added into Toyoura sand at different fines contents (FC) to form silty sands, which are denoted by TSS with a number indicating the fines content (e.g., TSS10 is the silty sand with FC = 10%). Noting that the sand and the silt are different in particle shape, a recent study [51] has shown that the particle shape of the base sand and the particle size disparity are two major factors controlling the cyclic behavior and resistance of silty sands, while the particle shape of fines appears to play a negligible role. The particle size distribution curves of the tested materials are presented in Fig. 2, and the basic properties of these materials are summarized in Table 1.

2.2. Testing procedures

Cyclic triaxial tests were conducted on specimens prepared by different sample preparation methods. The moist tamping and dry deposition methods were adopted to prepare specimens (diameter = 71.1 mm, height = 142.2 mm) with different soil fabrics. For the moist tamping method, the sand was uniformly mixed with water at a water content of 5% by mass. Then, a pre-determined amount of wet sand was poured into the split mold and compacted with a metal tamper to a prescribed layer height. The mold was filled with six layers of compacted sand. For the dry deposition method, oven-dried sand with a pre-determined mass was deposited into the split mold using a funnel. The funnel tip was maintained at a minimal height of drop above the sand surface, aiming to minimize the deposition potential energy to achieve a minimum possible density. Denser states of the specimen can be achieved by taping the periphery of the mold uniformly.

Noting that the degree of saturation significantly influences the liquefaction behaviors soils [52,53], two-stage saturation procedures were performed. The first stage is the percolation of CO₂ followed by the circulation of de-aired water. In the second stage, the specimens were further saturated by increasing the back pressure to at least 300 kPa or achieving a B value of at least 0.98. After the specimens were fully saturated, they were consolidated to the desired stress state. In triaxial tests, the stress state on the maximum shear stress plane (the inclined plane with an angle of 45° to the horizontal plane) is used to simulate the stress state on the horizontal plane of a soil element that is subjected to seismic loading. The specimen was consolidated isotropically and anisotropically for a stress state with zero and non-zero initial static shear stress, respectively. In particular, anisotropic consolidation was achieved by increasing the axial and radial stresses in small increments, maintaining a constant stress ratio until the desired stress condition was reached. The initial static shear stress ratio, α , is defined by the following equation for the triaxial condition,

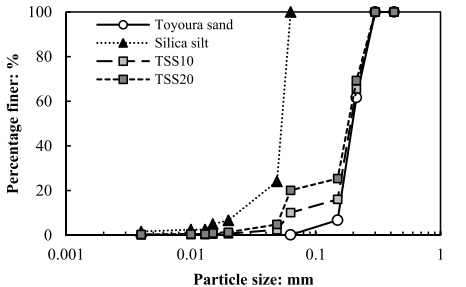




Fig. 2. Particle size distribution and SEM images of the tested materials.

Table 1Material properties.

Material	Mean particle size, D_{50}	Coefficient of uniformity, $C_{\rm u}$	Coefficient of curvature, C_c	Specific gravity, G_s
	(mm)	(-)	(-)	(-)
Toyoura sand	0.199	1.367	0.962	2.64
Crushed silica silt	0.053	2.176	1.765	2.65

$$\alpha = \frac{q_s}{2\sigma'_{nc}} = \frac{\sigma'_{1c} - \sigma'_{3c}}{\sigma'_{1c} + \sigma'_{3c}} \tag{1}$$

where q_s is the initial static deviatoric shear stress; $\sigma'_{nc} = (\sigma'_{1c} + \sigma'_{3c})/2$, is the post-consolidation effective normal stress on the maximum shear stress plane of the specimen, after consolidation; σ'_{1c} and σ'_{3c} are the post-consolidation axial and radial effective stresses, respectively. The mean effective stress after consolidation (p'_c) can be calculated based on the prescribed value of α and σ'_{nc} using the following equation

$$p_c' = \left(1 - \frac{\alpha}{3}\right)\sigma_{nc}' \tag{2}$$

After consolidation, sinusoidal deviatoric stress cycles with an amplitude of $q_{\rm cyc}$ were applied to the specimen under undrained condition. The amplitude of the cyclic loading is characterized by the cyclic shear stress ratio, *CSR*, defined as follows.

$$CSR = \frac{q_{cyc}}{2\sigma'_{uc}} \tag{3}$$

The testing program (Table 2) covered a range of fines contents (FC = 10% and 20%), packing density (post-consolidation void ratio, $e_c \approx 0.920$ –0.680), effective confining pressure ($\sigma'_{nc} = 40$ –300 kPa), and initial static shear stress ratio ($\alpha = 0$ –0.4).

3. Cyclic failure characteristics

3.1. Typical failure patterns

The typical failure patterns can be categorized into three general types, namely flow-type failure, cyclic mobility, and strain accumulation. The flow-type failure can be further divided into two sub-types, namely unlimited flow failure and limited flow failure. The packing density of the specimen is one of the major factors affecting the failure patterns.

For specimens at a very loose state, unlimited flow failure may take place. Fig. 3(a) presents the test result of a typical unlimited flow failure for a specimen with $e_c = 0.906$ and $\alpha = 0$. The three plots in Fig. 3(a) are the stress-strain relationship $(q-\varepsilon_a)$, stress path in the q-p' plane, and excess pore water pressure (Δu) generation with the number of stress cycles (N). The unlimited flow failure, once triggered, is characterized by a rapid increase of the axial strain to a very large level ($\varepsilon_a > 20\%$), while no significant accumulation of the pre-failure axial strain is observed ($\varepsilon_a < 5\%$). It is also observed that the excess pore water pressure developed with cyclic loading until a certain level that triggers the flow failure. For the case shown in Fig. 3(a), Δu increases to the effective confining pressure causing zero effective stress after the rapid flow deformation of the specimen. Fig. 3(b) presents one more example of unlimited flow failure for a loose specimen ($e_c = 0.907$), but with $\alpha =$ 0.4. Similarly, the specimen only developed a limited level of excess pore pressure and a small level of axial strain before the flow was triggered, but the axial strain developed to a level exceeding the limit of the apparatus ($\varepsilon_a > 20\%$) suddenly resulting in a zero effective stress in the end. The small pre-failure strain accumulation and limited pore pressure generation make the unlimited flow failure difficult to be monitored and

Table 2
Testing program.

Material	FC	SPM	e	$\sigma'_{ m nc}$	α	Test purpose
	%			kPa		
TSS10	10	Moist	0.910	100	0	CRR + failure
		tamping				pattern
			0.903	100,	0, 0.1,	CRR + failure
				300	0.25, 0.4	pattern
			0.873	100	0, 0.4	Failure
						pattern only
			0.861	100	0.25, 0.4	Failure
						pattern only
			0.858	100	0	Failure
						pattern only
			0.847	100	0, 0.1,	CRR + failure
					0.25, 0.4	pattern
			0.837	100	0.4	Failure
						pattern only
			0.791	40, 100,	0, 0.1,	CRR + failure
			0.515	300	0.25, 0.4	pattern
			0.717	100	0	CRR + failure
	10	Desc	0.847	100	0.01	pattern CRR + failure
	10	Dry	0.847	100	0, 0.1, 0.25	
		deposition	0.701	100	0.25	pattern CRR + failure
			0.791	100	0, 0.23,	pattern
			0.746	100	0.4	Failure
			0.740	100	Ü	pattern only
			0.717	100	0	Failure
			01, 1,	100	Ü	pattern only
			0.680	100	0	CRR + failure
						pattern
TSS20	20	Moist tamping	0.920	100	0	CRR + failure
						pattern
			0.903	100	0, 0.1,	CRR + failure
					0.25, 0.4	pattern
			0.847	100	0	CRR + failure
						pattern
			0.810	100	0	Failure
						pattern only
			0.791	40, 100,	0, 0.1,	CRR + failure
				300	0.25, 0.4	pattern
			0.727	100	0	Failure
						pattern only
			0.717	100	0	CRR + failure
		_	. = . :			pattern
	20	Dry	0.791	100	0, 0.1,	CRR + failure
		deposition	0.600	100	0.25	pattern
			0.680	100	0	CRR + failure
						pattern

forecasted, while the rapid flow deformation usually causes catastrophic consequences. A major difference between the failure characteristics of the two specimens in Fig. 3 is the direction of flow. For the specimen with $\alpha=0$, the specimen failed on the triaxial extension side, but the specimen with $\alpha=0.4$ failed on the triaxial compression side. This is due to biased cyclic stress caused by the presence of initial shear stress.

For relatively dense specimens, there are two types of failure patterns known as cyclic mobility and plastic strain accumulation, depending on the reversal conditions of the cyclic stress. Fig. 4(a) presents a specimen loaded by reversed stress cycles, exhibiting typical cyclic mobility. The excess pore pressure increases while the effective stress decreases cyclically until a state called "initial liquefaction" is reached, at which the effective stress transiently equals zero for the first time. The specimen undergoes two transient liquefaction states during each subsequent stress cycle when the deviatoric stress reverses its direction (i.e., q reaches zero), and large deformation takes place when the state of the specimen is reaching the transient liquefied state showing extremely low stiffness. Then, the stiffness and the strength of the specimen recovered due to dilation in the following loading process. Cyclic mobility can take place for either $\alpha=0$ or $\alpha\neq0$, as long as the cyclic stress reverses its direction (i.e., Fig. 1(c) and (d)). Fig. 4(b) presents an example of plastic

strain accumulation, which occurs if the cyclic stress does not reverse its direction (i.e., Fig. 1(e)). The major characteristic of this type of failure is the continuous accumulation of irrecoverable strain (i.e., plastic strain) in each stress cycle. The generation of excess pore pressure can be limited and the effective stress may not decrease to zero along with the loading cycles. For the specimen shown in Fig. 4(b), negative excess pore pressure was generated in the first a few stress cycles owing to dilation of the specimen.

The limited flow failure can take place in specimens with a packing density between the specimens shown in Figs. 3 and 4. The limited flow failure is also characterized by a small strain accumulation and cyclically increased pore pressure before triggering the flow deformation, similar to unlimited flow failure. Once the flow is triggered, the specimen deforms in a sudden and rapid way, but the deformation ceases after a certain level. Then, the specimen may exhibit cyclic mobility for specimens loaded with stress reversal (Fig. 5(a)) or plastic strain accumulation for specimens loaded without stress reversal (Fig. 5(b)).

3.2. Factors affecting failure patterns

In addition to the packing density, other factors, such as effective confining pressure and initial fabric, could also alter the failure pattern of the specimens. Fig. 6 presents an example that confining pressure can change the failure patterns. When the effective stress is 100 kPa, the TSS20 specimen with an initial void ratio of 0.796 exhibited plastic strain accumulation under the condition of $CSR = \alpha = 0.4$ (Fig. 6(a)). However, when the effective stress is 300 kPa, the TSS20 specimen with the same initial void ratio ($e_{\rm c} = 0.796$) exhibit flow-type failure for $\alpha = 0.4$, while CSR = 0.25 (Fig. 6(b)). This is because that increasing the confining pressure makes the specimen more contractive, and flow-type failure takes place when the specimen is at a more contractive state than those exhibit cyclic mobility or plastic strain accumulation.

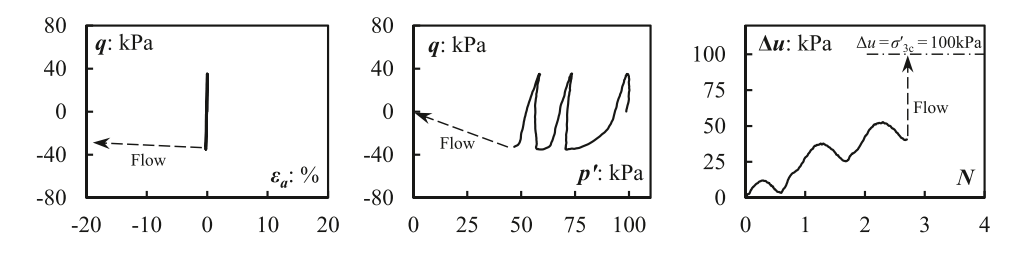
Fig. 7 presents an example that the failure pattern is affected by the loading condition (i.e., cyclic stress amplitude in this case). The two specimens with nearly the same void ratio ($e_c = 0.847$ and 0.849) were loaded by fully reversed stress cycles (i.e., $\alpha = 0$) with different *CSR*. For CSR = 0.15, cyclic mobility is observed as shown in Fig. 7(a), while for CSR = 0.2, limited flow failure takes place as shown in Fig. 7(b). The results from the two specimens indicate that the cyclic failure pattern can turn from a non-flow type (cyclic mobility in Fig. 7(a)) to a flow-type (limited flow in Fig. 7(b)) if the amplitude of cyclic loading increases. A similar observation has been reported by Chiaro et al. [19] based on strain-controlled cyclic torsional shear tests of TS with a relative density of around 50%.

The initial fabric induced by sample preparation methods can also change the failure patterns of the specimens. Examples are shown in Fig. 8. For the moist-tamped specimen with a post-consolidation void ratio of 0.795, the failure pattern is cyclic mobility when it was loaded under CSR = 0.3 (Fig. 8(a)). But, the specimen prepared by dry deposition exhibited limited flow (Fig. 8(b)) when loaded by stress cycles with CSR = 0.15. The dry-deposited specimen has a smaller cyclic resistance even if its void ratio is smaller than the moist-tamped specimen.

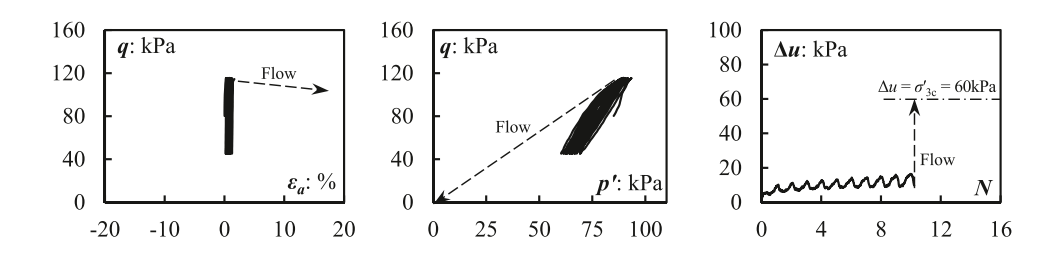
4. Cyclic resistance

4.1. Failure criteria and determination of cyclic resistance

Different failure patterns have been demonstrated in the previous section. Conventionally, excess pore water pressure is used to define failure since a high excess pore pressure is considered to be a typical feature of soil liquefaction due to cyclic loading. However, the present study and several recent studies observed that large deformation of specimens can take place even if the excess pore pressure remains at a relatively low level with the reference to the initial effective stress, particularly when the initial static shear stress is higher than the cyclic

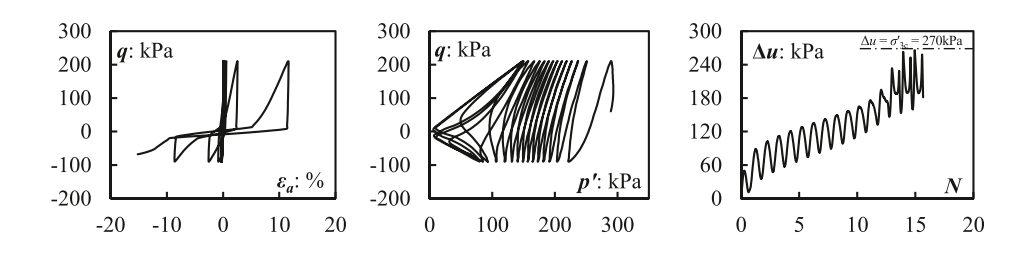


(a) TSS10, $e_c = 0.906$, $\alpha = 0$, $\sigma'_{nc} = 100$ kPa, CSR = 0.175

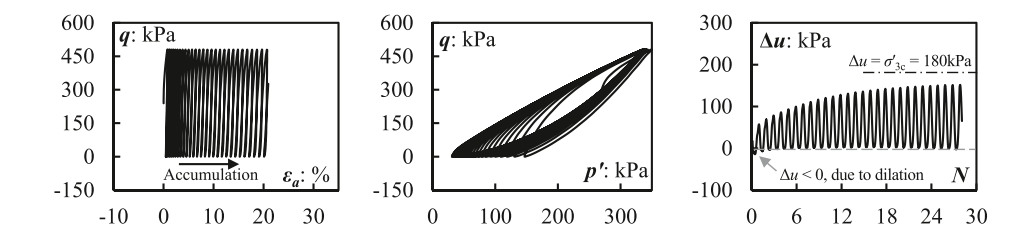


(b) TSS10, $e_c = 0.907$, $\alpha = 0.4$, $\sigma'_{nc} = 100$ kPa, CSR = 0.175

Fig. 3. Unlimited flow failure of specimens with and without initial static shear stress.



(a) Cyclic mobility for TSS10, $e_c = 0.795$, $\alpha = 0.1$, $\sigma'_{nc} = 300$ kPa, CSR = 0.25



(b) Plastic strain accumulation for TSS10, $e_c = 0.793$, $\alpha = 0.4$, $\sigma'_{nc} = 300$ kPa, CSR = 0.4

Fig. 4. Cyclic mobility and plastic strain accumulation of specimens loaded with and without stress reversal.

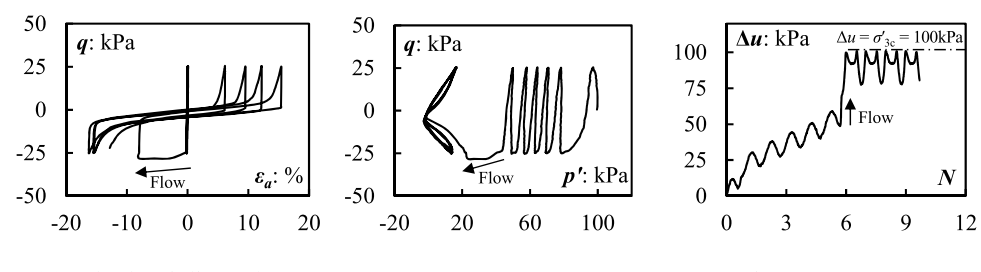
stress amplitude. In these cases, pore pressure-based criteria are no longer applicable. Instead, strain-based failure criteria can be applied to different cases. In the present study, the strain-based failure criteria are the onset of flow for specimens exhibiting flow-type failure, 5% double amplitude of axial strain for specimens exhibiting cyclic mobility, and 5% residual axial strain for specimens exhibiting cyclic plastic strain accumulation. It should be noted that the onset of flow is usually followed by a large strain development (e.g., unlimited flow failure), thus, the onset of flow is considered to be a simple and reasonable

representation of the strain-based failure.

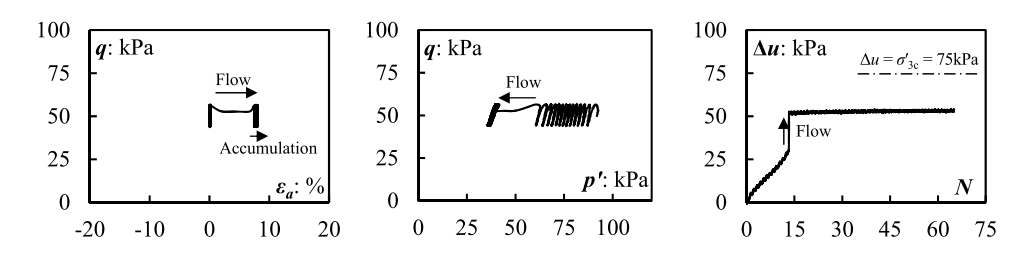
By applying stress cycles with different amplitudes, the specimens reached the failure state in different numbers of stress cycles. Fig. 9 presents typical *CSR-N*_I relationships, and the data are fitted by a power-law function showing as follows,

$$CSR = a(N_l)^b \tag{4}$$

where a and b are fitting parameters. The cyclic resistance ratio (CRR) of



(a) Limited flow for TSS10, $e_c = 0.778$, $\alpha = 0$, $\sigma'_{nc} = 100$ kPa, CSR = 0.125



(b) Limited flow for TSS10, $e_c = 0.828$, $\alpha = 0.25$, $\sigma'_{nc} = 100$ kPa, CSR = 0.03

Fig. 5. Limited flow failure of specimens with and without initial static shear stress.

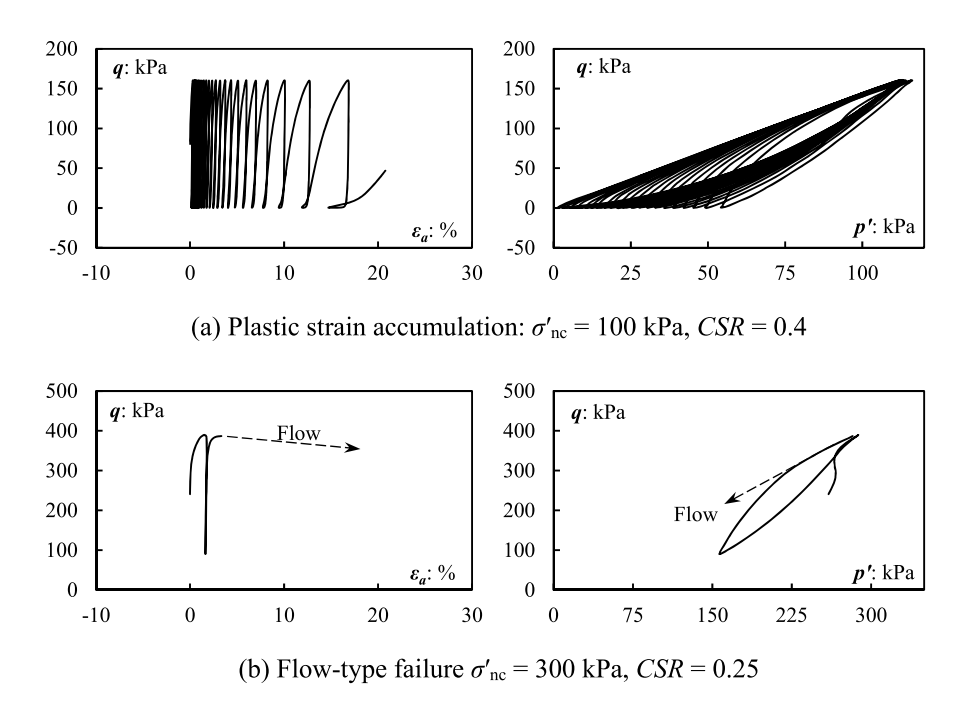


Fig. 6. Effect of confining stress on failure patterns (TSS20, $e_c = 0.796$, $\alpha = 0.4$).

the sand against soil liquefaction can be defined as the *CSR* causing liquefaction in a given number of cycles (e.g., $N_{\rm l}=10$ or 15), corresponding to the moment magnitude ($M_{\rm w}$) of an earthquake. For example, Idriss [54] suggested the mean number of equivalent uniform cycles is 10 and 15 for an earthquake with $M_{\rm w}=7$ and 7.5, respectively. In this study, $N_{\rm l}=10$ is used to define *CRR*, in agreement with several previous investigations (e.g., Refs. [2,51]).

4.2. Effects of initial states

It has been widely observed that the cyclic resistance ratio of sand depends on initial states, namely the void ratio and effective stress

before cyclic loading. The cyclic resistance of sands decreases with increasing void ratio, as shown in Fig. 10. It is also noted that these relationships are also affected by the initial static shear stress ratio and sample preparation method. The dry-deposited specimens are more susceptible to liquefaction than their moist-tamped counterparts when compared under otherwise similar conditions. For specimens prepared by moist tamping, the CRR_{10} -e relationships move upwards when α increased from 0 to 0.25. However, for specimens prepared by dry tamping, the specimens with $\alpha=0.25$ experienced a more significant decrease in cyclic resistance with increasing void ratio than those with $\alpha=0.25$

The cyclic resistance ratio decreases with increasing effective stress,

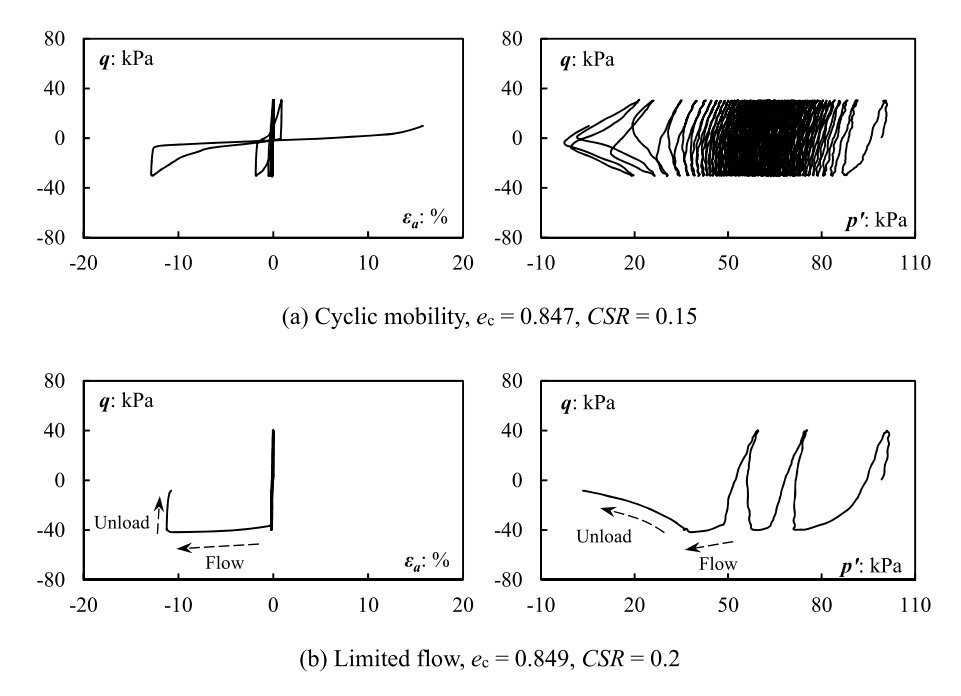


Fig. 7. Effect of *CSR* on failure patterns (TSS10, $e_c = 0.847-0.849$, $\alpha = 0$, $\sigma'_{nc} = 100$ kPa).

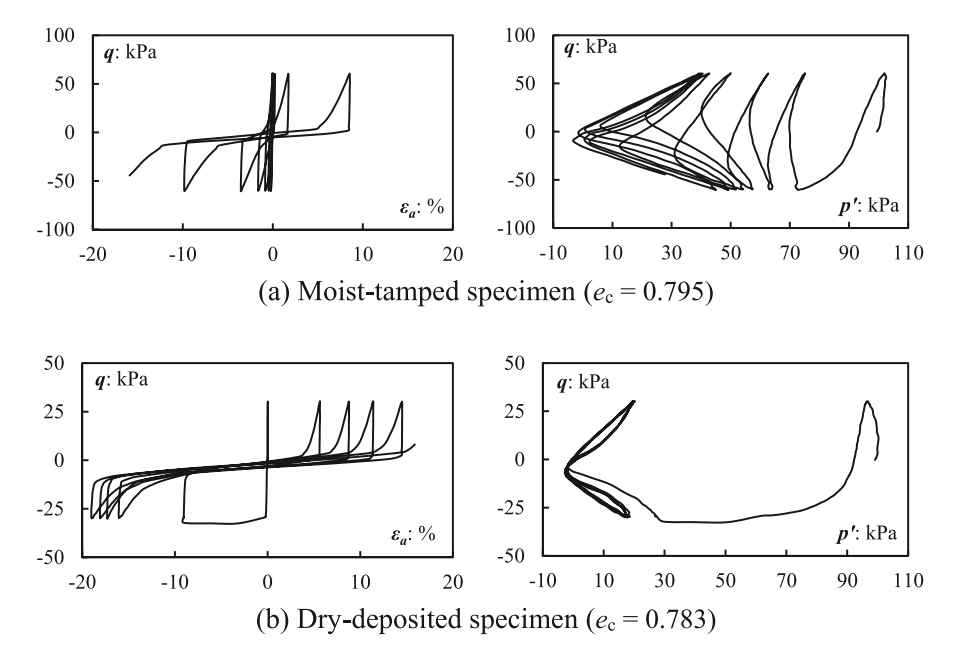


Fig. 8. Effect of fabric on failure patterns (TSS10, $\alpha = 0$, $\sigma'_{nc} = 100$ kPa).

and a stress correction factor, K_{σ} , is usually used for characterization. Hynes and Olsen [6] recommended using a power function to characterize the decrease of K_{σ} with increasing effective stress and suggested that denser specimens would experience a more severe decrease of CRR due to increased effective stress. Their proposal has been recommended by NCEER, however, it does not take into account non-zero α conditions. It has been consistently observed that initial static shear stress interplays with effective stress to influence the cyclic resistance of sands [3,25] (Fig. 11). In addition, soil fabric induced by sample preparation methods introduces additional complexity to the K_{σ} as revealed by Sze et al. [33]. For example, as shown in Fig. 11(b), the K_{σ} of the dry-deposited specimen with $D_r=35\%$ is significantly lower than that of the moist-tamped specimen for 500 kPa, but soil fabric has little impact on the K_{σ} of specimens with $D_r=50\%$.

4.3. Effects of initial static shear stress

The effects of initial static shear stress on the cyclic resistance ratio of clean and silty sands can be either beneficial or detrimental, depending on the void ratio and the effective stress [2,3]. Fig. 12(a) exhibits the CRR_{10} - α relationship for both moist-tamped and dry-deposited TSS10 specimens considering different void ratios. With increasing void ratio, the effect of initial static shear stress on cyclic resistance ratio turns from a purely positive effect to a negative effect with an initial positive effect at low α values. However, it should be noted that the dry-deposited specimens have lower cyclic resistance than the moist-tamped ones when compared under otherwise similar conditions. In addition, by comparing the moist-tamped specimens of void ratio around 0.847 and the dry-deposited specimens of void ratio around 0.819, it is found that

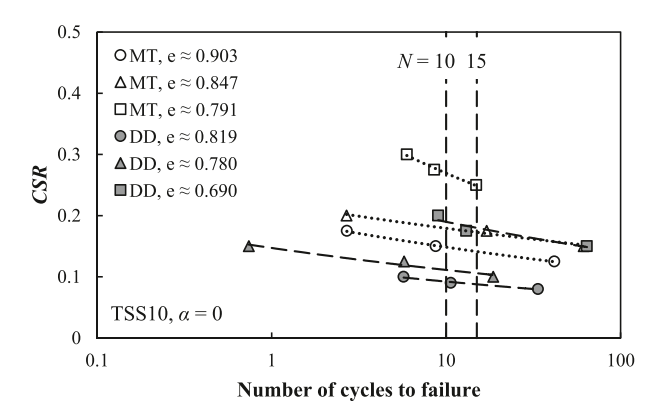


Fig. 9. Relationships between cyclic stress ratios and numbers of cycles to failure.

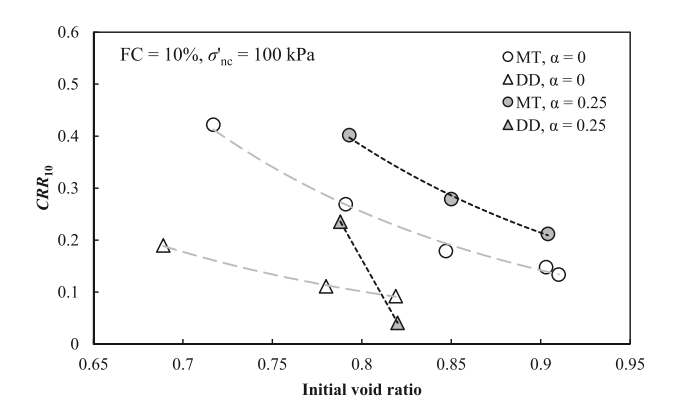


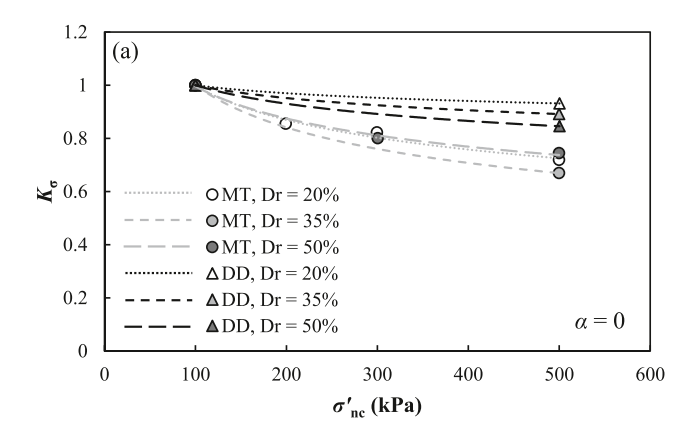
Fig. 10. Effect of void ratio on the cyclic resistance of silty sands.

effects of initial static shear stress are different for specimens with different initial fabrics. For the moist-tamped specimens (MT, $e \approx 0.847$), CRR increases monotonically with increasing α (0–0.4), but for the dry-deposited specimens (DD, $e \approx 0.819$), CRR first increases and then decreases with increasing α and the maximum CRR is obtained when $\alpha \approx 0.1$. Data considering the effects of effective stress on the CRR- α relationships can be found in previous investigations [2,3], indicating that increasing effective stress can turn a positive effect of α into a negative effect.

To characterize the effect of initial static shear, a correction factor, K_{α} , was introduced by Seed [4]. It is defined as follows.

$$K_{\alpha} = \frac{CRR_{\alpha \neq 0}}{CRR_{\alpha = 0}} \tag{5}$$

where $CRR_{\alpha\neq0}$ and $CRR_{\alpha=0}$ are cyclic resistance ratios under different α values but the same initial void ratio and effective stress. The K_{α} - α relationships are presented in Fig. 12(b) for both MT and DD TSS10 specimens considering different void ratios. For MT specimens, the K_{α} - α relationships for e=0.791 and 0.847 almost coincide with each other, but the K_{α} - α relationship for e=0.903 is different from the other two, showing a drop of K_{α} when $\alpha=0.2$. The result indicates the effects of void ratio on the correction factor K_{α} . In addition, the effect of sample preparation on K_{α} can also be found in Fig. 12(b) that the K_{α} - α relationship of DD specimens with e=0.783 is higher than that of the K_{α} - α relationship of DD specimens with e=0.819 is lower than that of K_{α} - α relationship of MT specimens with e=0.847.



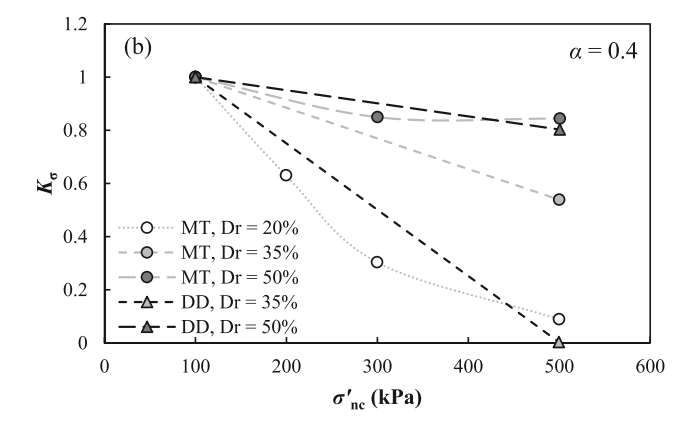


Fig. 11. Effects of sample preparation method and initial static shear stress on K_{σ} (Data adapted from Sze et al. (2022) for clean Toyoura sand).

5. Critical state-based characterizations

5.1. Characterization of failure patterns

Difficulties remain in the prediction of the failure pattern of a specimen due to complicated interactions among a variety of influencing factors. According to the aforementioned test results, the failure pattern turns from flow-type to non-flow type with decreasing void ratio or initial effective confining pressure. It could be helpful to characterize the state-dependent feature of the failure patterns through Been and Jefferies's state parameter concept [26], which measures the vertical distance between the initial state and the critical state line in the e-p' plane. The critical state lines of the TSS series have been reported in Ref. [47], which were obtained by monotonic triaxial tests. Fig. 13(a) presents an example using data of TSS20 that increase of void ratio and increase of effective stress turns failure patterns from cyclic mobility to flow-type failure for $\alpha = 0$. Fig. 13(b) converts the horizontal axis from void ratio to Been and Jefferies's state parameter [26]. It is found that the specimens with void ratios of around 0.794 and effective stress of 300 kPa have a larger state parameter than those specimens exhibiting cyclic mobility, suggesting that the change failure pattern is associated with the change of state parameter. In other words, the change of failure pattern is related to the change of dilative tendency, since the state parameter is representative of the dilatancy. Similarly, the failure patterns of TSS10 appear to be related to the state parameter, as shown in Fig. 13(c).

Fig. 14(a) compares the results of MT and DD specimens. Similarly, the failure patterns of DD specimens turn from cyclic mobility to flow-type failure with increasing state parameters. But, it is noted that the range of states of limited flow for the DD specimen is much wider than that for MT specimens, and the DD specimens can exhibit flow failure at states where MT specimens exhibited cyclic mobility. For initial

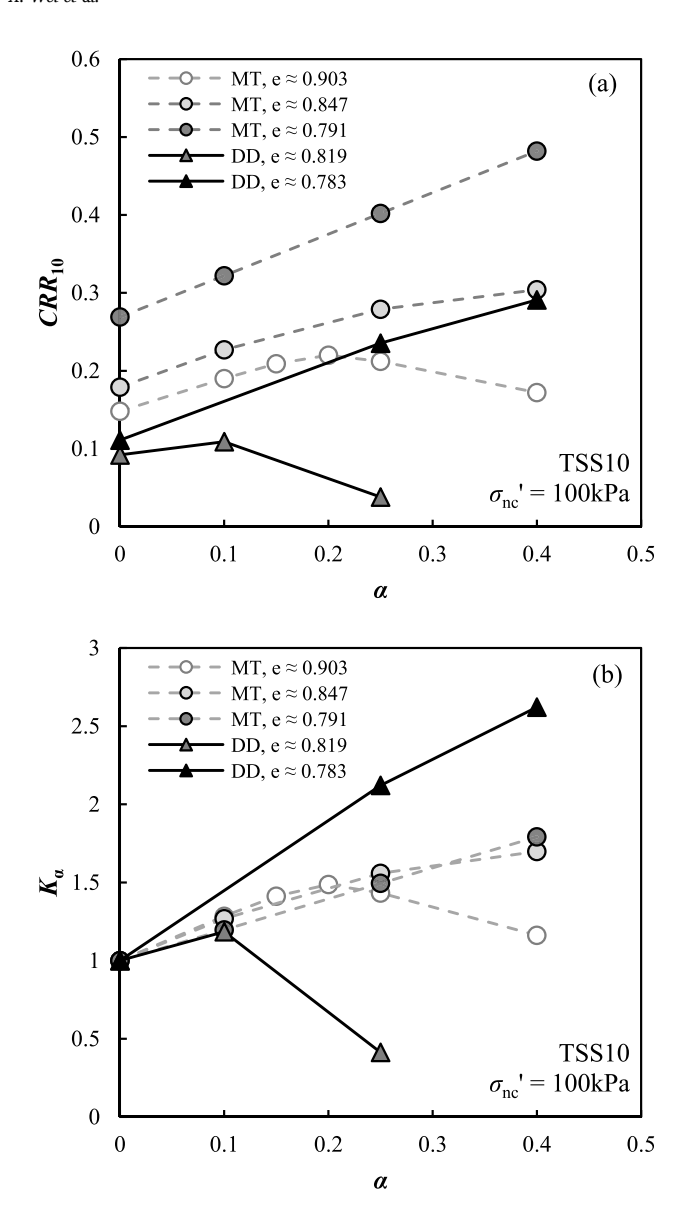
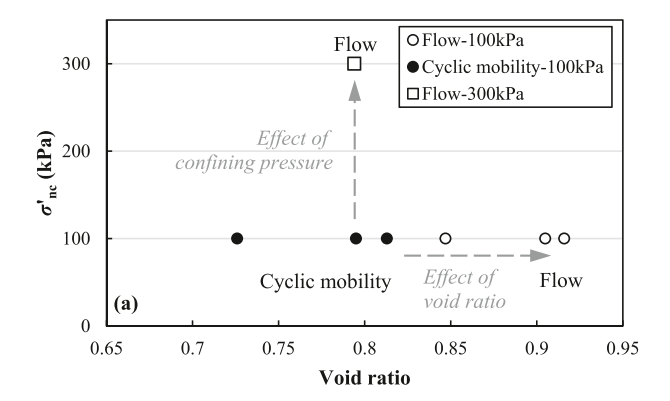


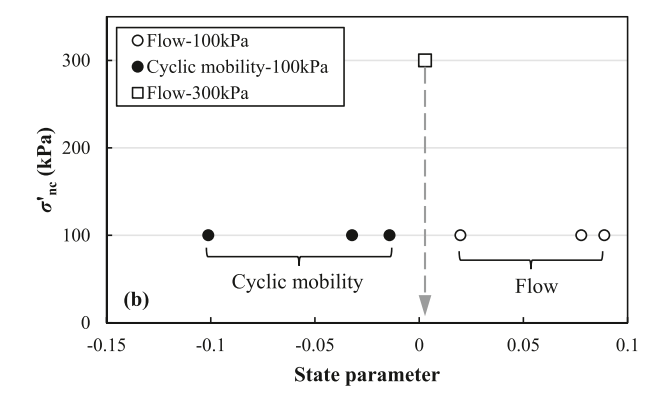
Fig. 12. Effects of initial static shear stress ratio on cyclic resistance and K_{α} correction factor.

conditions with the initial static shear stress, the cyclic failure pattern also turns from flow type (white data points) to non-flow type (black data points) with decreasing state parameter, as shown in Fig. 14(b) for TSS10. The non-flow type failure patterns are cyclic mobility and plastic strain accumulation depending on the reversal condition of the cyclic loading. In Fig. 14(b), several data points are filled with the grey color denoting transition states, at which these specimens can either exhibit flow or non-flow type failure depending on the amplitude of cyclic stress.

5.2. Evaluation of cyclic resistance

Several previous investigations indicated that the state parameter can be used to establish a critical state-based framework that characterizes the effects of void ratio and the effective stress on the liquefaction resistance of sands [2,3,43] in a unified way. One of the advantages of the state parameter-based framework is the capability to unify different material properties such as fines content and particle characteristics [47,51]. In addition, the effects of the initial static shear stress can also be taken into account in this framework as demonstrated by Refs. [2,3].





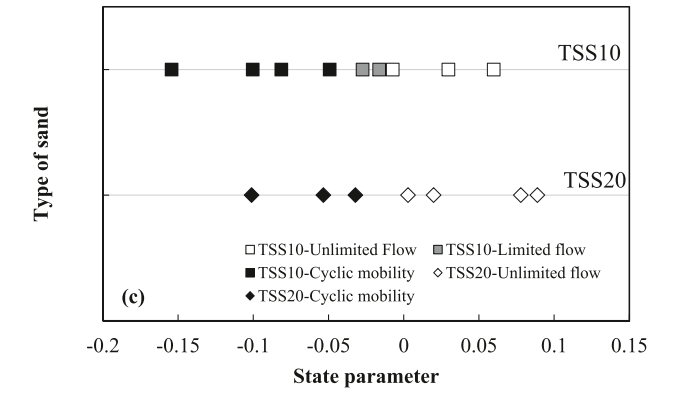
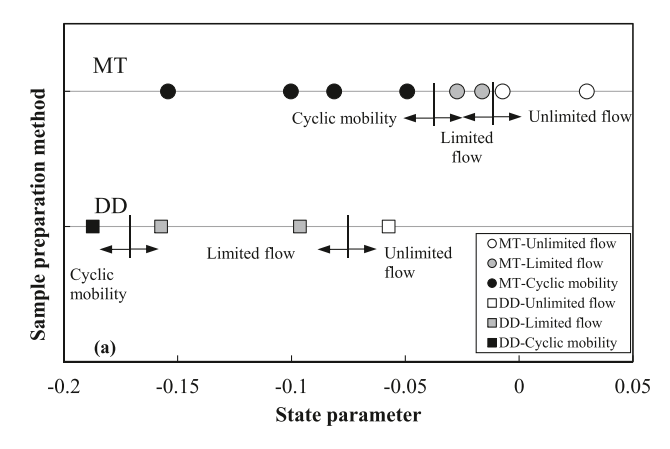


Fig. 13. Effects of initial state on the failure patterns.

Fig. 15 presents test data considering different initial states (i.e., void ratio and effective stress) and initial static shear stress ratios for the clean and silty sands. The grey lines were provided by Yang and Sze [2, 24] for MT TS specimens which are also capable of characterizing the cyclic resistance ratio of MT silty sands [3]. The data points in Fig. 15 are the test data for the DD clean and silty sands, and the black trend lines are the best-fitting lines for these data points. For each initial static shear stress ratio, the cyclic resistance ratio decreases with increasing state parameters in a unified way, and there appears to be no impact of fines on the CRR_{10} - ψ relationships. Similar to the findings for MT specimens [3,24], the linear CRR_{10} - ψ relationships are subjected to a clockwise rotation with increasing α . However, it should be noted that the CRR_{10} - ψ relationships are different for the DD and MT specimens under otherwise similar conditions. The following linear equation is used to characterize the CRR_{10} - ψ relationship for each α ,

$$CRR_{10} = -c \cdot \psi + d \tag{6}$$



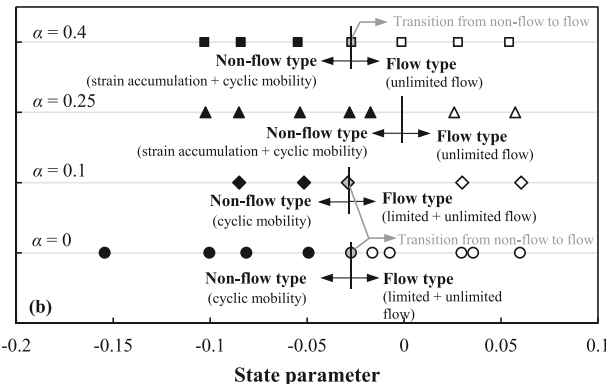


Fig. 14. Effects of fabric and initial static shear stress on the state-dependence of failure patterns for TSS10.

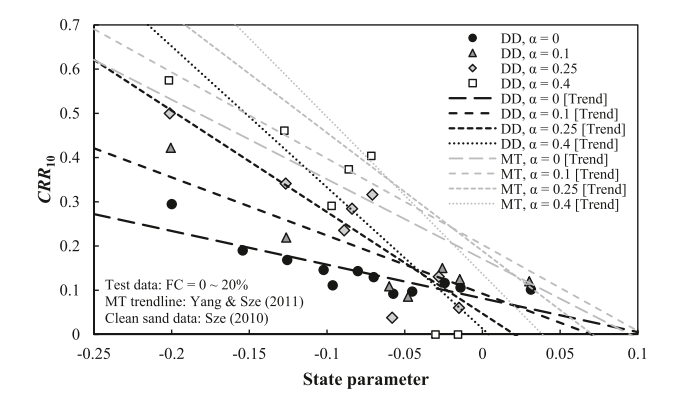


Fig. 15. CRR_{10} - ψ relationships for MT and DD specimens.

where c and d are fitting parameters. Parameters c and d are functions of initial static shear stress ratio (Fig. 16) that parameter c increases with increasing α while parameter d first increases and then decreases with increasing α . The trends of different sample preparation methods are different as a result of different soil fabrics.

6. Discussion

6.1. Critical state-based failure pattern prediction

The present study proposed a conceptual framework to predict the cyclic failure patterns for sands, by establishing the correlation between the initial state parameter with the failure patterns. There appears to be

a clear trend that the cyclic failure pattern gradually turns from non-flow type to flow-type with increasing state parameters, for each initial static shear stress and soil fabric. Although state boundaries separating the failure patterns were given in the study, more test data are still needed to confirm the conceptual framework and to precisely locate the boundaries. In addition, the conceptual framework did not take into account the effects of loading amplitude on the failure patterns, and thus, problems can be encountered when the state of the specimen is at the transition from the non-flow to flow-type. For example, the specimen can exhibit cyclic mobility when it is loaded with stress cycles of smaller amplitudes but flow-type failure when it is loaded with stress cycles of higher amplitudes. Moreover, the proposed method also needs to be validated by using other types of sands. In addition, it is also of interests to extend the critical state framework for a wider range of cyclic behaviors of sands (e.g., rheological characteristics [55,56]).

6.2. Implications of the CRR- ψ framework to the conventional evaluation procedures

The cyclic resistance can be conventionally calculated through the following equation for a given initial state (i.e., void ratio and effective stress) and initial shear stress.

$$CRR_{\sigma \neq 100kPa,\alpha \neq 0} = K_{\alpha}K_{\sigma}CRR_{\sigma = 100kPa,\alpha = 0}$$
(7)

where $\mathit{CRR}_{\sigma \neq 100 kPa,~\alpha \neq 0}$ is the cyclic resistance ratio at any effective stress and initial static shear stress; $\textit{CRR}_{\sigma \ = \ 100 \text{kPa}, \ \alpha \ = \ 0}$ is the cyclic resistance ratio at effective stress of 100 kPa without any initial static shear stress, which can be obtained from the liquefaction resistance assessment charts. However, it remains ambiguous regarding how to obtain the two correction factors, K_{α} and K_{σ} . Fig. 17 presents an example to illustrate how to apply the *CRR-\psi* correlation to estimate the K_{α} and K_{σ} . To estimate the $CRR_{\sigma \neq 100 \text{kPa}, \ \alpha \neq 0}$ for given effective stress (e.g., 300 kPa), initial static shear stress ratio (e.g., $\alpha = 0.4$), and a soil with a known void ratio (e.g., e_0), the first step is to estimate the $CRR_{\sigma=100\text{kPa}}$. $\alpha = 0$ under an initial state with effective stress of 100 kPa and that void ratio, e_0 . The void ratio of e_0 and the stress state of 100 kPa result in a state parameter of ψ_1 , while the void ratio of e_0 and the stress state of 300 kPa result in a state parameter of ψ_2 . To emphasize the importance of proper selection of the correction factors, a special case is assumed that the *CRR*- ψ correlations for $\alpha = 0$ and 0.4 have an intersect at a state parameter between ψ_1 and ψ_2 . Two possible approaches to calculate the desired CRR for a specimen with the initial condition (e_0 , 300 kPa, $\alpha =$

Approach I (Fig. 17(a)).

(1) Convert $CRR_{\sigma=100\text{kPa},~\alpha=0}$ to $CRR_{\sigma=300\text{kPa},~\alpha=0}$ by multiplying the K_{σ} at 300 kPa for $\alpha=0$ ($K_{\sigma=100\text{kPa},~\alpha=0}$), i.e., following CRR- ψ for $\alpha=0$.

$$CRR_{\sigma=300kPa,\alpha=0} = K_{\sigma=300kPa,\alpha=0}CRR_{\sigma=100kPa,\alpha=0}$$
 (8)

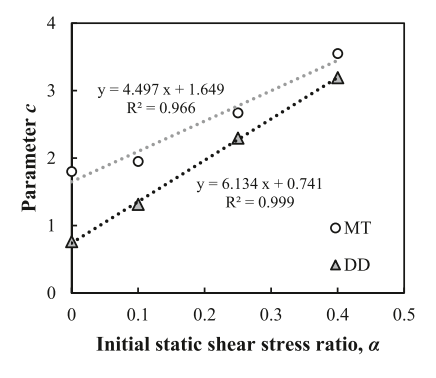
(2) The overburden corrected cyclic resistance ratio, $CRR_{\sigma=300\text{kPa},\ \alpha}$ $_{=\ 0}$, needs to be corrected for initial static shear stress. Since the cyclic resistance has been corrected for overburden pressure, the state parameter of the specimen has already changed to ψ_2 (= ψ_1 + $\Delta \psi$). The correction factor K_{α} should take the value at the state parameter of ψ_2 (i.e., $K_{\alpha,\ w2}$) instead of ψ_1 ($K_{\alpha,\ w1}$).

$$CRR_{\sigma=300kPa,\alpha=0.4} = K_{\alpha,\psi}, CRR_{\sigma=300kPa,\alpha=0}$$

$$\tag{9}$$

Notes: If K_{α} for ψ_1 (K_{α, ψ_1}) is used in the second step, the cyclic resistance will be overestimated because K_{α} for ψ_1 is higher than that for ψ_2 .

Approach II (Fig. 17(b)).



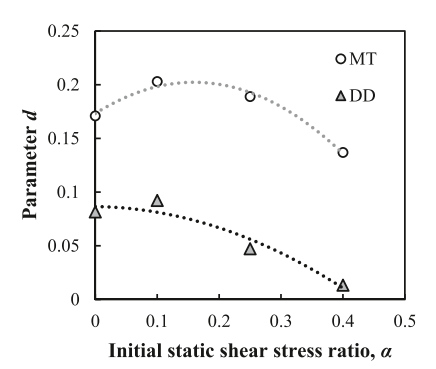
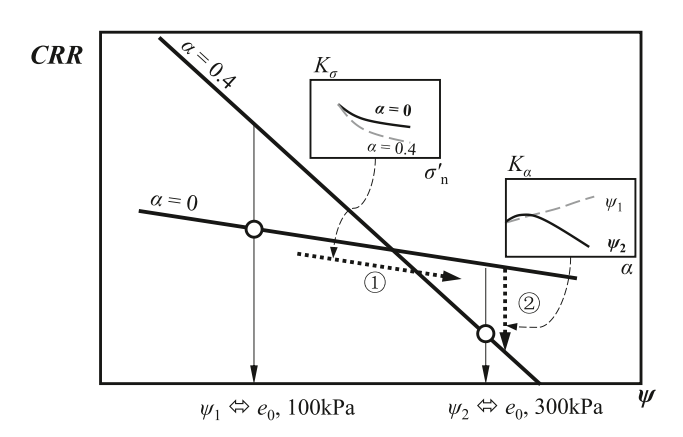
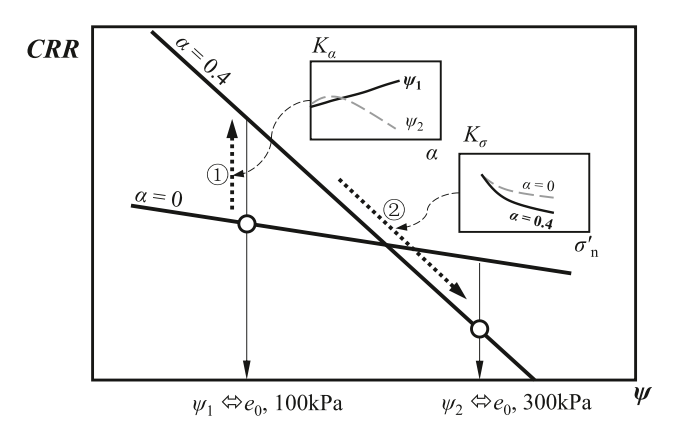


Fig. 16. Effects of initial static shear stress on the linear fitting parameters of CRR_{10} - ψ relationships.



(a) Approach I



(b) Approach II

Fig. 17. Schematic diagrams of the $\mathit{CRR-\psi}$ framework-based approaches to predicting the cyclic resistance ratio.

(1) Convert $CRR_{\sigma=100\text{kPa},\ \alpha=0}$ to $CRR_{\sigma=100\text{kPa},\ \alpha=0.4}$ by multiplying the K_{α} at ψ_1 for $\alpha=0.4$.

$$CRR_{\sigma=100kPa,\alpha=0.4} = K_{\alpha,\psi_1}CRR_{\sigma=100kPa,\alpha=0}$$
 (10)

(2) The cyclic resistance ratio is further corrected by considering the effects of effective stress with $\alpha = 0.4$.

$$CRR_{\sigma=300kPa,\alpha=0.4} = K_{\sigma=300kPa,\alpha=0.4}CRR_{\sigma=100kPa,\alpha=0.4}$$
(11)

Notes: If K_{σ} for 100 kPa is used in the second step, the cyclic resistance ratio will be overestimated.

The proposal of using the two correction factors (i.e., K_{α} and K_{σ}) is to simplify the estimation of cyclic resistance from a perspective of empiricism. However, uncertainties remain when determining the two factors and may mislead engineering practice. The illustrations in Fig. 17 indicates that the state dependence of K_{α} and K_{σ} should not be ignored, and proper selection of the K_{α} and K_{σ} value is also crucial to a safe design.

6.3. Limitations of the CRR-\u03c4 framework

The CRR-\psi framework suggested a promising way to evaluate the liquefaction resistance of sand with a variety of influencing factors in a unified way, including packing density, effective stress, and soil properties (e.g., fines content, particle shape). It also complies with the conventional liquefaction evaluation procedures, by suggesting statedependent correction factors for initial static shear stress and effective overburden pressure. This study has shown that the cyclic resistance of sand can be affected by soil fabric for a given packing density, effective stress, and initial static shear stress. So, it is important but difficult to replicate the in-situ fabric in the laboratory to carefully calibrate the CRR-\psi framework. In addition, the fabric can be influenced by the deposition process of soil, stress history, liquefaction history, etc. Investigations through particle-scale perspectives [57,58] may help to incorporate fabric effects into the critical state framework. For instance, Gu et al. [57] proposed a micro state parameter considering the mechanical contacts between sand particles and suggested it to be particularly useful to unify the cyclic resistance of specimens with the same state parameter but formed by different methods.

7. Conclusions

This study investigated the effects of initial states, initial static shear stress, and soil fabric on the cyclic behavior and liquefaction resistance of silty sands. The major findings are given as follows.

- Four major cyclic failure patterns are identified, including two nonflow type (i.e., cyclic mobility and plastic strain accumulation) and two flow-type (i.e., unlimited flow and limited flow) failure patterns.
 The cyclic failure patterns are dependent on the void ratio, effective stress, initial static shear stress, loading amplitude, and soil fabric.
- 2. For a given soil fabric and initial static shear stress ratio, the failure patterns of sand gradually turn from non-flow type to flow-type, suggesting that the state of soil plays an important role in governing the cyclic failure patterns. The state boundaries separating the failure patterns are dependent on the soil fabric and the initial static shear stress ratio.

- 3. The soil fabric can affect the cyclic resistance ratio of silty sands. It also affects the stress correction factor, K_{σ} , and the initial shear correction factor K_{σ} , suggesting further investigations are still needed for the effects of overburden pressure and initial shear with consideration of soil fabric.
- 4. The CRR- ψ relationships are also proposed for silty sands with different soil fabrics. Clockwise rotation of the linear CRR- ψ relationships with increasing α is confirmed for silty sand with different soil fabrics.
- 5. By using the $CRR-\psi$ framework, recommendations for the conventional liquefaction assessment are provided regarding the applications of K_{σ} and K_{α} corrections.

Author statement

Xiao Wei: Methodology; Investigation; Writing- Original draft. Zhongxuan Yang: Writing- Review & editing.

Jun Yang: Conceptualization, Methodology; Investigation; Supervision; Funding acquisition; Writing-review & editing.

Declaration of competing interest

The authors declare that they have no known competing financial interests or personal relationships that could have appeared to influence the work reported in this paper.

Data availability

Data will be made available on request.

Acknowledgment

This study is supported by the Key Research and Development Program of Zhejiang Province (No. 2022C03180), the Research Grants Council of Hong Kong (No. 17206418; No. C7038-20G), National Natural Science Foundation of China (No. 52108351), and the Fundamental Research Funds for the Central Universities (2021QNA4021, 2021FZZX001-14).

References

- Ishihara K. Liquefaction and flow failure during earthquakes. Geotechnique 1993; 43:351–451.
- [2] Yang J, Sze HY. Cyclic behaviour and resistance of saturated sand under nonsymmetrical loading conditions. Geotechnique 2011;61:59–73.
- [3] Wei X, Yang J. Cyclic behavior and liquefaction resistance of silty sands with presence of initial static shear stress. Soil Dynam Earthq Eng 2019;122:274–89.
- [4] Seed HB. Earthquake-resistant design of earth dams. Int Conf Recent Adv Geotech Earthq Eng Soil Dyn 1981:1157–73.
- [5] Olsen RS. Liquefaction analysis using the cone penetrometer test. In: 8th world conf earthq eng, vol. III; 1984. p. 247–54.
- [6] Hynes ME, Olsen RS. Influence of confining stress on liquefaction resistance. Int Work Phys Mech Soil Liq 1999:145–52.
 [7] Boulanger RW. High overburden stress effects in liquefaction analyses. J Geotech
- [7] Boulanger RW. High overburden stress effects in liquefaction analyses. J Geotech Geoenviron Eng 2003;129:1071–82.
- [8] Pan K, Xu TT, Liao D, Yang ZX. Failure mechanisms of sand under asymmetrical cyclic loading conditions: experimental observation and constitutive modelling. Geotechnique 2022;72:162–75.
- [9] Boulanger RW. Relating $K\alpha$ to relative state parameter index. J Geotech Geoenviron Eng 2003;129:770–3.
- [10] Mohamad R, Dobry R. Undrained monotonic and cyclic triaxial strength of sand. J Geotech Eng 1986;112:941–58.
- [11] Sze HY, Yang J. Failure modes of sand in undrained cyclic loading: impact of sample preparation. J Geotech Geoenviron Eng 2014;140:152–69.
- [12] Park S-S, Nong Z-Z, Lee D-E. Effect of vertical effective and initial static shear stresses on the liquefaction resistance of sands in cyclic direct simple shear tests. Soils Found 2020;60:1588–607.
- [13] Yang ZX, Pan K. Flow deformation and cyclic resistance of saturated loose sand considering initial static shear effect. Soil Dynam Earthq Eng 2017;92:68–78.
- [14] Pan K, Yang ZX. Effects of initial static shear on cyclic resistance and pore pressure generation of saturated sand. Acta Geotech 2018;13:473–87.
- [15] Castro G. Liquefaction of sands. Harvard University; 1969.

- [16] Vaid YP, Chern JC. Effect of static shear on resistance to liquefaction. Soils Found 1983;23:47–60.
- [17] Robertson PK, Fear CE. Liquefaction of sands and its evaluation. In: Ishihara K, editor. 1st int. Conf. Earthq. Geotech. Eng. Tokyo, Japan: Balkema; 1995. p. 1253–87. Rotterdam.
- [18] Tomasello G, Porcino DD. Influence of sloping ground conditions on cyclic liquefaction behavior of sand under simple shear loading. Soil Dynam Earthq Eng 2022;163:107516.
- [19] Chiaro G, Koseki J, Kiyota T. New insights into the failure mechanisms of liquefiable sandy sloped ground during earthquakes. In: 6th int. Conf. Earthq. Geotech. Eng.; 2015. p. 200. Christchurch, New Zealand.
- [20] Yoshimi Y, Oh-Oka H. Influence of degree of shear stress reversal on the liquefaction potential of saturated sand. Soils Found 1975;15:27–40.
- [21] Seed RB, Harder Jr LF. SPT-based analysis of cyclic pore pressure generation and undrained residual strength. H Bolt Seed Meml Symp 1990;2:351–73.
- [22] Harder Jr LF, Boulanger R. Application of $K\sigma$ and $K\alpha$ correction factors. NCEER Work Eval Liq Resist Soils 1997:129–48.
- [23] Youd T, Idriss I, Andrus R, Arango I, Castro G, Christian J, et al. Liquefaction resistance of soils: summary report from the 1996 NCEER and 1998 NCEER/NSF workshops on evaluation of liquefaction resistance of soils. J Geotech Geoenviron Eng 2001;127:817–33.
- [24] Yang J, Sze HY. Cyclic strength of sand under sustained shear stress. J Geotech Geoenviron Eng 2011;137:1275–85.
- [25] Vaid YP, Stedman JD, Sivathayalan S. Confining stress and static shear effects in cyclic liquefaction. Can Geotech J 2001;38:580–91.
- [26] Been K, Jefferies MG. A state parameter for sands. Geotechnique 1985;35:99–112.
- [27] Arthur JRF, Menzies BK. Inherent anisotropy in a sand. Geotechnique 1972;22: 115–28.
- [28] Oda M. Initial fabrics and their relations to mechanical properties of granular material. Soils Found 1972;12:17–36.
- [29] Yang ZX, Li XS, Yang J. Quantifying and modelling fabric anisotropy of granular soils. Geotechnique 2008;58:237–48.
- [30] Tatsuoka F, Ochi K, Fujii S, Okamoto M. Cyclic undrained triaxial and torsional shear strength of sands for different sample preparation methods. Soils Found 1986;26:23–41.
- [31] Kuerbis R, Vaid YP. Sand sample preparation-theslurry deposition method. Soils Found 1988;28:107–18.
- [32] Tatsuoka F, Muramatsu M, Sasaki T. Cyclic undrained stress-strain behaviour of dense sand by torsional simple shear. Soils Found 1982;22:55–70.
- [33] Sze HY, Wei X, Yang J. Fabric anisotropy and overburden pressure effects on liquefaction resistance. In: Proc. 20th int. Conf. Soil mech. Geotech. Eng.; 2022. Sydney. Australia.
- [34] Cubrinovski M, Bray JD, Taylor M, Giorgini S, Bradley B, Wotherspoon L, et al. Soil liquefaction effects in the central business district during the February 2011 Christchurch earthquake. Seismol Res Lett 2011;82:893–904.
- [35] Yasuda S, Harada K, Ishikawa K, Kanemaru Y. Characteristics of liquefaction in tokyo bay area by the 2011 great east Japan earthquake. Soils Found 2012;52: 793–810.
- [36] Wei X, Guo Y, Yang J, Guo C. Liquefaction characteristics of four Ya-An low-plastic silty sands with presence of initial static shear stress. In: Qiu T, Tiwari B, Zhang Z, editors. Proc. GeoShanghai 2018 int. Conf. Adv. Soil dyn. Found. Eng. Shanghai: Springer; 2018. p. 62–9. Singapore.
- [37] Mason HB, Gallant AP, Hutabarat D, Montgomery J, Reed AN, Wartman J. Geotechnical reconnaissance: the 28 september 2018 M7.5 palu-donggala, Indonesia earthquake, 2019.
- [38] Shen CK, Vrymoed JL, Uyeno CK. The effects of fines on liquefaction of sands. 9th Int Conf Soil Mech Found Eng 1977:381–6.
- [39] Kuerbis RH, Negussey D, Vaid YP. Effect of gradation and fines content on the undrained response of sand. A Spec Conf Hydraul Fill Struct 1988:330–45.
- [40] Carraro JAH, Bandini P, Salgado R. Liquefaction resistance of clean and nonplastic silty sands based on cone penetration resistance. J Geotech Geoenviron Eng 2003; 129:965–76.
- [41] Xenaki VC, Athanasopoulos GA. Liquefaction resistance of sand-silt mixtures: an experimental investigation of the effect of fines. Soil Dynam Earthq Eng 2003;23: 1–12
- [42] Dash HK, Sitharam TG. Undrained cyclic pore pressure response of sand-silt mixtures: effect of nonplastic fines and other parameters. Geotech Geol Eng 2009; 27:501–17.
- [43] Stamatopoulos CA. An experimental study of the liquefaction strength of silty sands in terms of the state parameter. Soil Dynam Earthq Eng 2010;30:662–78.
- [44] Mele L, Lirer S, Flora A. Evaluation of cyclic resistance and postliquefaction volumetric strains of intermediate soils. J Geotech Geoenviron Eng 2022;148: 06022009.
- [45] Porcino DD, Diano V. The influence of non-plastic fines on pore water pressure generation and undrained shear strength of sand-silt mixtures. Soil Dynam Earthq Eng 2017;101:311–21.
- [46] Polito CP, Martin JR. Effects of nonplastic fines on the liquefaction resistance of sands. J Geotech Geoenviron Eng 2001;127:408–15.
- [47] Wei X, Yang J. Characterizing the effects of fines on the liquefaction resistance of silty sands. Soils Found 2019;59:1800–12.
- [48] Thevanayagam S. Effect of fines and confining stress on undrained shear strength of silty sands. J Geotech Geoenviron Eng 1998;124:479–91.
- [49] Wei X, Yang J, Zhou Y-G, Chen Y. Influence of particle-size disparity on cyclic liquefaction resistance of silty sands. Géotech Lett 2020;10:155–61.

- [50] Pan K, Zhou GY, Yang ZX, Cai YQ. Comparison of cyclic liquefaction behavior of clean and silty sands considering static shear effect. Soil Dynam Earthq Eng 2020; 139:106338.
- [51] Wei X, Yang J. Characterising the effect of particle size disparity on liquefaction resistance of non-plastic silty sands from a critical state perspective. Geotechnique 2021;73:323–36.
- [52] Yang J, Savidis S, Roemer M. Evaluating liquefaction strength of partially saturated sand. J Geotech Geoenviron Eng 2004;130:975–9.
- [53] Zhang N, Liu X, Lan H. Characterizing saturation state of loess using P-wave velocity. Eng Geol 2021;290:106207.
- [54] Idriss IM. An update to the Seed-Idriss simplified procedure for evaluating liquefaction potential. TRB Work New Approaches to Liq 1999.
- [55] Tong LH, Qi B, Xu C. Fluidity characteristic of granular materials within low frequency dynamics. Int J Mech Sci 2021;202–203:106508.
- [56] Mele L. An experimental study on the apparent viscosity of sandy soils: from liquefaction triggering to pseudo-plastic behaviour of liquefied sands. Acta Geotech 2022;17:463–81.
- [57] Gu X, Zhang J, Huang X. DEM analysis of monotonic and cyclic behaviors of sand based on critical state soil mechanics framework. Comput Geotech 2020;128: 103787.
- [58] Huang X, Xu M, Zhang Z, Lei Q. Characterizing stress variability within granular samples upon liquefaction. Comput Geotech 2020;127:103771.